Journal of Hazardous Materials 166 (2009) 1120–1126

Contents lists available at ScienceDirect

Journal of Hazardous Materials

journal homepage: www.elsevier.com/locate/jhazmat

Molecular based equation of state for shocked liquid nitromethane

Nicolas Desbiens*, Emeric Bourasseau, Jean-Bernard Maillet, Laurent Soulard

Département de Physique Théorique et Appliquée, Commissariat à l'Energie Atomique, Centre DAM - Ile de France, Bruyères-le-Châtel, 91297 Arpajon, France

ARTICLE INFO

Article history:
Received 20 October 2008
Received in revised form 2 December 2008
Accepted 2 December 2008
Available online 25 December 2008

Keywords:
Monte Carlo molecular simulation
Equation of state
Nitromethane
Hugoniot
Derivative properties

ABSTRACT

An approach is proposed to obtain the equation of state of unreactive shocked liquid nitromethane. Unlike previous major works, this equation of state is not based on extended integration schemes [P.C. Lysne, D.R. Hardesty, Fundamental equation of state of liquid nitromethane to 100 kbar, J. Chem. Phys. 59 (1973) 6512]. It does not follow the way proposed by Winey et al. [J.M. Winey, G.E. Duvall, M.D. Knudson, Y.M. Gupta, Equation of state and temperature measurements for shocked nitromethane, J. Chem. Phys. 113 (2000) 7492] where the specific heat C_v, the isothermal bulk modulus B_T and the coefficient of thermal pressure $(\partial P/\partial T)_V$ are modeled as functions of temperature and volume using experimental data. In this work, we compute the complete equation of state by microscopic calculations. Indeed, by means of Monte Carlo molecular simulations, we have proposed a new force field for nitromethane that lead to a good description of shock properties [N. Desbiens, E. Bourasseau, J.-B. Maillet, Potential optimization for the calculation of shocked liquid nitromethane properties, Mol. Sim. 33 (2007) 1061; A. Hervouët, N. Desbiens, E. Bourasseau, J.-B. Maillet, Microscopic approaches to liquid nitromethane detonation properties, J. Phys. Chem. B 112 (2008) 5070]. Particularly, it has been shown that shock temperatures and second shock temperatures are accurately reproduced which is significative of the quality of the potential. Here, thermodynamic derivative properties are computed: specific heats, Grüneisen parameter, sound velocity among others, along the Hugoniot curve. This work constitutes to our knowledge the first determination of the equation of state of an unreactive shocked explosive by molecular simulations.

1. Introduction

Shock to detonation transition in explosives is a complex and poorly understood phenomenon which has been initially described by Chaiken for liquid explosives [1–3]. Briefly, the propagation of a shock wave in the fresh explosive brings the system onto a particular point of its Hugoniot curve, the ZND state. After an induction time, exothermic decomposition occurs rapidly in the shocked matter. The kinetic of the decomposition follows the Arrhenius law, implying a strong temperature dependence [4,5]. Determination of shock temperatures, and more usually of a complete equation of state (EOS) of an unreactive explosive, then appears as a key point for predicting the first step of the shock to detonation transition. Unfortunately, determination of shock temperatures based on Raman scattering [6–8], on pyrometry [9] or radiance spectra measurements [10,11] are scarce. As a consequence, the simplest solution to circumvent this problem consists in using generalized equations of state based on some experimental data [12,7]. Such approximations are of great importance in the quality of the prediction of shocked state temperature, for example, which is crucial for thermally activated processes such as chemical reactions. Although the quantities calculated by the EOS of Lysne and Hardesty [12] and Winey et al. [7] are qualitatively similar, they can show some important discrepancies, particularly in their derivative properties (up to 50% for the Grüneisen ratio). As mentioned by Winey et al. [7] and Desbiens et al. [13], an adequate test for evaluating an EOS is the prediction of shock temperatures. In this paper, we will compare unceasingly our results to those of Lysne and Hardesty [12] and Winey et al. [7].

In order to provide some informations to the reader about the equations of state proposed by Lysne and Hardesty [12] and Winey et al. [7], we briefly describe here their methods. The approach of Lysne and Hardesty is based on a partial EOS $e(p, v)$ obtained from a continuum of Hugoniots centered at different known initial states (thermodynamic description of the 1 atm isobar). The complete EOS $e(s, v)$ is then determined by numerical solution of two differential equations governing entropy and temperature along the Hugoniot. Winey et al. developed a complete EOS by use of Hugoniot data and isotherm data. C_v is modeled as a single Einstein oscillator using isobaric data and Raman data under shock conditions. $(\partial P/\partial T)_V$ is calculated from thermodynamic relationships, Hugoniot, isothermal and isobaric data. The isothermal compressibility

* Corresponding author. Tel.: +33 1 69 26 68 09.
E-mail addresses: nicolas.desbiens@cea.fr (N. Desbiens), emeric.bourasseau@cea.fr (E. Bourasseau), jean-bernard.maillet@cea.fr, laurent.soulard@cea.fr (L. Soulard).

0304-3894/$ – see front matter © 2008 Elsevier B.V. All rights reserved.
doi:10.1016/j.jhazmat.2008.12.083

Table 1
Internal geometry of nitromethane.

Bond lengths and angle	
d_{N-O} (Å)	1.225
d_{N-CH_3} (Å)	1.70584
$O\hat{N}O$ (°)	125.0

β_T is calculated from thermodynamic relationships, isothermal and isobaric data. Then these three quantities are sufficient to build the complete EOS.

In our work, no assumption is made on the evolution of thermodynamical quantities. Instead, the system is described by microscopic methods: interatomic interactions and Monte Carlo molecular simulations. Then, using statistical mechanics, all thermodynamical quantities of interest can be extracted. The present paper describes in a first part the force field used to model the nitromethane interactions which has been the subject of a previous paper [13]. This section also focuses on the accuracy of the prediction of single and multiple shock temperatures with a slight description of the methods (more details are provided in Refs. [13] and [14]). The second part is devoted to the computation of derivative properties, and thus a complete tabulated EOS of unreacted shocked liquid nitromethane is proposed.

2. Force field of nitromethane and methods

2.1. Force field

Since under high pressures (up to 20 GPa) the variations of covalent bond lengths in nitromethane are limited to 3.5% [15], we chose to fix the internal geometry of the molecule. The chosen bond lengths and bond angles are taken from previous force fields [16,17] and are reported in Table 1[13].

The force field is composed of an electrostatic part and a repulsion–dispersion part acting on the nitrogen and oxygen atoms and on the CH_3 group described as a pseudo-atom following the idea of Ungerer et al. [17] for petroleum fluids. The functional forms of these interactions are indicated in equation (1) where σ corresponds to the minimum of the repulsion–dispersion form, $-\varepsilon$ is the minimal energy and α is a measure of the steepness of the repulsion part of the potential. The values of the atomic or pseudo-atomic parameters are reported in Table 2 and cross parameters are obtained through Lorentz–Berthelot rules [13]:

$$U(r_{ab}) = \frac{q_a q_b}{r_{ab}} + \frac{\epsilon_{ab}}{\alpha_{ab} - 6}\left[6\,e^{\alpha_{ab}(1-((r_{ab})/(\sigma_{ab})))} - \alpha_{ab}\left(\frac{\sigma_{ab}}{r_{ab}}\right)^6\right] \quad (1)$$

The values reported in Table 2 have been obtained by means of a home-made optimization procedure using a random exploration of the parameter space. This procedure consists in choosing some random values for the different parameters of the force field (in a physical range) and then computing some physical quantities. Then a comparison is made between the computed quantities and the reference data available through the use of an error function. The aim is to minimize this error function. In this case, the force field has been optimized on three experimental reference data, namely the density of liquid at the initial state (300 K and 1 atm), the vaporization enthalpy at the initial state and the pressure on a point of the Hugoniot provided by B. Crouzet et al. [18]. The values of the electrostatic charges are chosen by using the average *ab initio* charges on N, O and CH_3 calculated on different configurations of liquid nitromethane at 300 K between 0.9 and 1.6 g cm^{-3} [19]. Details about the optimization procedure can be found in Ref. [13].

Table 2
Values of the parameters of the force field (Eq. (1)).

	σ (Å)	ϵ (K)	α	q ($\lvert e\rvert$)
N	3.287	59.32	15.08	+0.54
O	2.797	95.49	12.40	−0.37
CH_3	4.531	99.16	13.12	+0.20

This force field has been shown to accurately reproduce the Hugoniot curve in a (P– v) diagram. Moreover second shock temperatures are also in good agreement with experimental data whereas temperatures are not included into the optimization process [13]. As pointed out by Liu et al. [20], nitromethane has been the subject of numerous studies (at ambient conditions, at high pressures and temperatures and along the Hugoniot) performed with various complex potentials including intramolecular and intermolecular interactions [20–28]. Politzer et al. studied the properties of nitromethane at ambient and high pressures [25,26]. Liquid and solid properties of nitromethane at ambient and high pressure have been investigated by Thompson et al. [21–24]. Jones used a perturbation theory coupled with an exponential-6 potential to study the Hugoniot properties of nitromethane but the computed shock temperatures clearly differ from the experiments [27]. Soulard calculated Hugoniot curves based on classical molecular dynamics simulations but the computed shock temperatures are substantially lower than the experimental ones [28]. Finally, Liu et al. [20] used the force field developed by Politzer et al. to study nitromethane under shock conditions. They showed that shock pressures and temperatures obtained with this force field are markedly different from experimental results. As a consequence, to our knowledge no force field of the literature is known to reproduce accurately shock temperatures.

2.2. Hugoniot curve

The so-called Hugoniot curve is the ensemble of accessible states that a system can reach after a shock from an initial state. The thermodynamic quantities of a material in the initial unshocked state and in the final shocked state are linked by the Rankine-Hugoniot conservation relations of mass, momentum and energy (Eqs. (2)–(4)). In these relations, P is the pressure, v is the specific volume ($\rho = 1/v$), e is the specific energy, D is the shock velocity and u is the particle velocity:

$$\rho_0 \cdot D = \rho \cdot (D - u) \quad (2)$$

$$P - P_0 = D \cdot u \cdot \rho_0 \quad (3)$$

$$Hg = e - e_0 - \frac{1}{2} \cdot (P + P_0) \cdot (v_0 - v) = 0 \quad (4)$$

Subscript '0' corresponds to material in the initial state.

In order to compute the Hugoniot curve, we employed the Adaptive Erpenbeck-Equation Of State (AE-EOS) method previously detailed in Ref. [29] and initially proposed by Brennan et al. [30]. This method is based on a succession of simulations carried out at constant number of molecules N, volume V and temperature T (NVT) [13,29].

Starting from an instantaneously compressed initial configuration, the system is simulated in the canonical ensemble (NVT_1) and the Hugoniot difference Hg_1 is computed by averaging over several hundred of thousand iterations (typically 500,000 in our case). The Hg term measures the gap between the simulated thermodynamic state and the real Hugoniot state. Then, the temperature of the system is slightly modified from T_1 to T_2 (∼10 K). During the following 500,000 iterations, Hg_2 is evaluated. At the end of this second stage, the derivative

$$\frac{dHg}{dT}(2) = \frac{Hg_1 - Hg_2}{T_1 - T_2}$$

is calculated. From here, the new temperature of the system T_3 is determined through

$$T_3 = T_2 - \frac{Hg_2}{(\mathrm{d}Hg/\mathrm{d}T)(2)}$$

and the simulation NVT_3 is performed for 500,000 iterations, during which Hg_3 is computed. This process is automatically iterated every 500,000 steps, evaluating each time

$$\frac{\mathrm{d}Hg}{\mathrm{d}T}(n) = \frac{Hg_{n-1} - Hg_n}{T_{n-1} - T_n}$$

and the new temperature is

$$T_{n+1} = T_n - \frac{Hg_n}{(\mathrm{d}Hg/\mathrm{d}T)(n)}$$

Temperature is iterated until the required accuracy on Hg (which has to be equal to zero) is obtained. Once the Hugoniot temperature T_{hug} is reached, an additional NVT_{hug} simulation can be performed to compute accurately the Hugoniot pressure P_{hug}.

2.3. Derivative properties

Quantities such as the isothermal compressibility β_T or the specific heat at constant volume C_v, which are second order derivatives of the Gibbs energy, can be computed by means of statistical fluctuations [31,32].

These calculations are based on the derivation of the partition function of the system which leads to:

$$\left.\frac{\partial < X >}{\partial T}\right|_P = \frac{< X \cdot \hat{H} > - < X >< \hat{H} >}{kT^2} \quad (5)$$

$$\left.\frac{\partial < X >}{\partial P}\right|_T = \frac{< X >< V > - < X \cdot V >}{kT} \quad (6)$$

where V is the volume, $\hat{H} = U_{ext} + U_{int} + P \cdot V$ is the configurational enthalpy, U_{ext} is the intermolecular interaction energy, U_{int} is the intramolecular one. The enthalpy H equals to $\hat{H} + K$ where K is the kinetic energy. For example, the coefficient of thermal expansion α_P reads

$$\alpha_P = \frac{1}{< V >} \cdot \left.\frac{\partial < V >}{\partial T}\right|_P = \frac{< V \cdot \hat{H} > - < V >< \hat{H} >}{< V > kT^2} \quad (7)$$

Isentropic quantities can even be calculated by use of thermodynamical identities: the Grüneisen parameter Γ (which is the negative slope of the isentrope in $\log T - \log V$ plane) or the adiabatic exponent γ_{ad} (which is the negative slope of the isentrope in $\log P - \log V$ plane) [33]. Details about this efficient method can be found in Refs. [31] and [32].

2.4. Taking into acount the intramolecular interactions

The intramolecular energy of the model we developed is constant. However for thermodynamic quantities such as specific heats, entropy or specific energy (see Eq. 4), vibrational motions have to be taken into account. This is done by using the Burcat's thermodynamic tables for ideal gas [34]. This stage, not described here for clarity, is explained in Ref. [29].

3. Results

3.1. Hugoniot curve of unreacted nitromethane

In this work, we have computed the Hugoniot properties for 38 values of specific volume (and the initial state). These values are regularly spaced by 0.01 $\mathrm{cm^3\,g^{-1}}$, starting from the specific volume

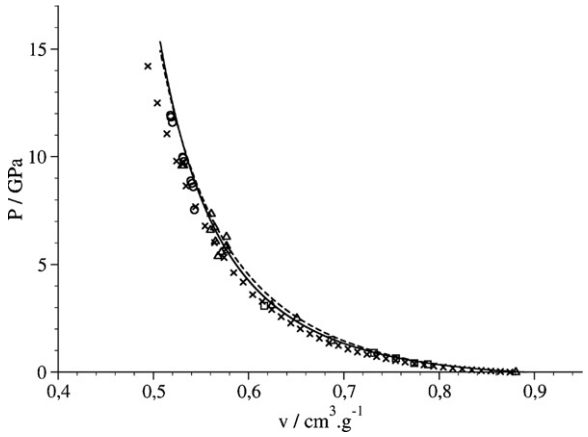

Fig. 1. P–v Hugoniot curve of unreacted nitromethane. Open symbols correspond to experimental results: circles: Crouzet et al. [9]; squares: Klébert [37]; triangles: Marsh [36]. Lines correspond to EOS of the literature: line: Lysne and Hardesty [12]; dashed line: Winey et al. [7]. Crosses correspond to our Monte Carlo (MC) simulation results.

of the initial state (0.8741 $\mathrm{cm^3\,g^{-1}}$). For every point (except the initial state), we have performed a NVT AE-EOS simulation in order to determine the pressure and the temperature on the Hugoniot. The method used here is exactly the same as in Ref. [13]. The physical quantities are computed by block averages [35] and statistical uncertainties on physical quantities are computed by usual errors propagation laws. Except if explicitly mentioned, the uncertainties are of the size of the symbols.

The pressure vs specific volume curve obtained by simulation is reported in Fig. 1 and compared to experimental and numerical data. We mention here that for all the following figures, the legend is splitted in open symbols for experimental values, line and dashed line for EOS of the literature (line for Lysne and Hardesty [12] and dashed line for Winey et al. [7]) and crosses for our simulation results. As expected and as detailed in Refs. [13] and [14], the agreement between the experimental values, the EOS of the literature and our own results is satisfactory.

The D-u curve, obtained by means of Eqs. (2) and (3) and reported in Fig. 2, is also in good accordance with the experimental results of Marsh [36] and Klébert [37].

More interestingly, and as previously mentioned in Ref. [13], shock temperatures and second shock temperatures are accurately reproduced. Fig. 3, which displays pressure vs temperature, confirms this conclusion. The same findings can be drawn for the temperature vs volume relation (see Fig. 4). Experimental results

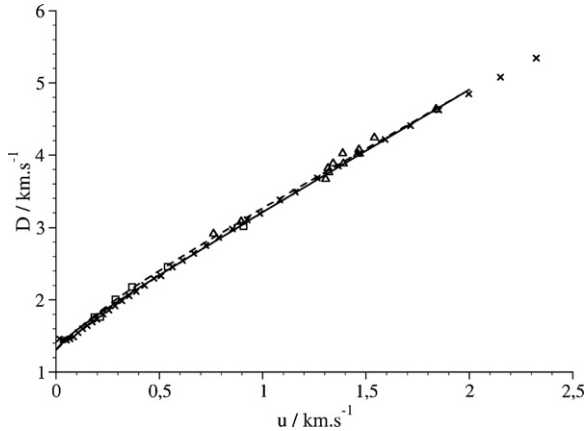

Fig. 2. D–u Hugoniot curve of unreacted nitromethane. Squares: Klébert [37]; triangles: Marsh [36]. Same legend as Fig. 1.

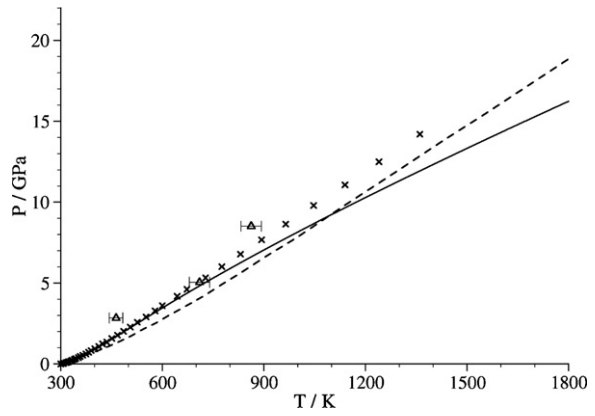

Fig. 3. P– T Hugoniot curve of unreacted nitromethane. Triangles: Delpuech et al. [6,8]. Same legend as Fig. 1.

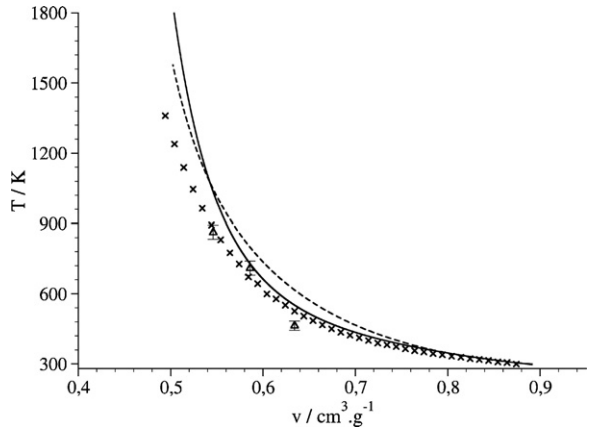

Fig. 4. T–v Hugoniot curve of unreacted nitromethane. Triangles: Delpuech et al. [6,8]. Same legend as Fig. 1.

of first and second shock are compared to simulation results in Table 3.

3.2. Derivative properties along the Hugoniot

In this section are detailed the simulated derivative properties as a function of the specific volume. The heat capacity at constant volume C_v, the sound velocity C_s and the Grüneisen parameter Γ are firstly depicted since these quantities are usually used as input for hydrodynamics codes. Indeed, from these quantities, shock temperatures can be determined.

Table 3
Comparison of experimental and simulation results of first and second shock. For first shock properties, comparisons of temperatures are made for the same pressure whereas for second shock properties, comparisons of pressure and temperature are made for the same compression (v/v_0).

	P (GPa)	T (K)
First shock		
Exp. [6,8]	2.8 ± 0.1	474 ± 24
This work	2.8	544
Exp. [6,8]	5.0 ± 0.2	712 ± 35
This work	5.0	702
Exp. [6,8]	8.5 ± 0.4	865 ± 43
This work	8.5	949
Second shock		
Exp. of Crouzet [13]	14.6	980 ± 50
This work	16.13 ± 0.04	1057

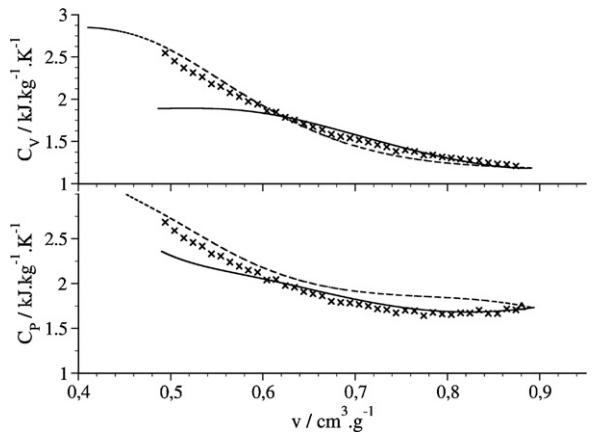

Fig. 5. Heat capacities at constant volume C_v and constant pressure C_p along the Hugoniot. Triangle: Jones and Giauque [38], and Berman and West [39]. Same legend as Fig. 1. Simulation uncertainties mentioned in text.

3.2.1. Heat capacities at constant volume C_v and constant pressure C_p

The evolution of the heat capacity at constant volume obtained by the EOS of the literature, reported in Fig. 5, shows a sigmoidal shape. The value of C_v increases notably at ~0.75 $cm^3\ g^{-1}$. The EOS of Lysne and Hardesty [12] and Winey et al. [7] are in good agreement for low compressions ($v > 0.6\,cm^3\,g^{-1}$) but below $0.6\,cm^3\,g^{-1}$ an increasing discrepancy appears. The values of C_v differ up to ~30% at $0.5\,cm^3\,g^{-1}$. As it can be seen on Fig. 5, our simulation results are consistent with the EOS of Winey et al.

We also present in Fig. 5 the results concerning the heat capacity at constant pressure C_p compared to experimental data of Jones and Giauque [38] and Berman and West [39] and to the EOS of the literature (where C_p is deduced from other derivative properties). The relative statistical uncertainty on our results decreases from 3.6% to 1.4% for C_v when specific volume decreases and from 1.6% to 0.9% for C_p. These uncertainties are relatively small. One can note that the C_p curves of the EOS tend to display small waves, this behaviour is to our opinion quite unphysical and may be due to accumulation of uncertainties in the numerical procedure. On the contrary, the simulated curve has the same convexity along the Hugoniot. It appears in Fig. 5 that our simulation results rather agree with the EOS of Lysne and Hardesty at low pressures (v greater than $0.6\,cm^3\,g^{-1}$) and agree with the EOS of Winey et al. at high pressures (v lower than $0.6\,cm^3\,g^{-1}$). Other quantities such as the Grüneisen parameter will shed light on this behaviour.

3.2.2. Sound velocity C_s

The sound velocity is reported in Fig. 6 with statistical uncertainties decreasing from 2.3% to 0.8%. Simulation results are in good agreement with the EOS of Lysne and Hardesty [12] and Winey et al. [7] up to 0.55 $cm^3\,g^{-1}$; nevertheless below $0.55\,cm^3\,g^{-1}$, the discrepancy seems to increase as the compression increases. The simulated sound velocity at initial state ($1274\,m\,s^{-1}$) is close to the experimental one ($1301\,m\,s^{-1}$ [12]) since the relative difference is of 2%.

3.2.3. Grüneisen parameter Γ

The shape of the Grüneisen parameter curve obtained by simulation is merely convex (reported in Fig. 7) with statistical uncertainties decreasing from 5.5% to 4.2%. Uncertainties are again quite small and enable to make a pertinent comparison between our results and the EOS of the literature. On the contrary, the Grüneisen parameter curves obtained from the EOS present two extrema: a maximum around ~0.8 $cm^3\ g^{-1}$ and a minimum around 0.5–0.6 $cm^3\,g^{-1}$. It is clear that the values of Γ dramatically differ

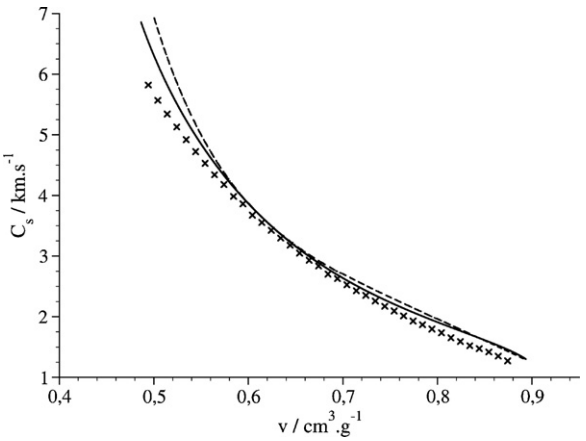

Fig. 6. Sound velocity along the Hugoniot. Same legend as Fig. 1. Simulation uncertainties mentioned in text.

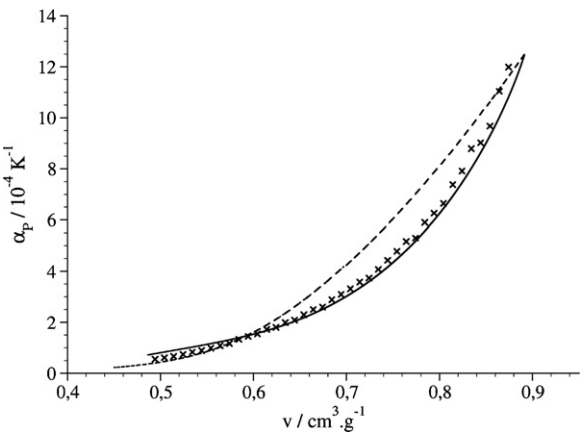

Fig. 8. Coefficient of thermal expansion along the Hugoniot. Same legend as Fig. 1.

from one EOS to the other. Winey et al. argued that this shape is due to a competition between the behaviour of $(\partial P/\partial T)_V$ which is mainly dominated by its volume dependence and the behaviour of C_v which is dominated by its temperature dependence (since $\Gamma/v = (\partial P/\partial T)_V/C_v$) [7]. Nonetheless, as previously discussed by Bridgman [40], $(\partial P/\partial T)_V$ fails to be a function of volume only when compared to experiments and the deviation does not seem to be negligible. Moreover $(\partial P/\partial T)_V$ tends to decrease with increasing temperature at constant volume. These arguments are also admissible to justify the shape of our own curve. In this situation, a deeper investigation of the behaviour of these thermodynamical quantities both experimentally and by simulation would be of great interest. Finally, we want to point out that we are quite confident in our simulations results mainly for two reasons. The transferability of the potential used in the work has been checked, this force field is able to reproduce second shock temperatures although it has not been optimized on such experimental data [13]. Whatever the conditions imposed (pressure and temperature) the way used to compute the independent derivative properties and the accuracy on these properties is the same. On the contrary, although the EOS of Winey et al. gives accurate second shock temperatures, the EOS of the literature make use of integration schemes, these procedures can probably accumulate errors, especially for the derivative properties.

3.2.4. Coefficient of thermal expansion α_P

The coefficient of thermal expansion is reported in Fig. 8. Our result match the EOS of Lysne and Hardesty [12] while the EOS of Winey et al. provides higher values of α_P (up to 30%) above 0.6 $cm^3\ g^{-1}$. Nonetheless, the global shapes are consistent. Once again, experimental data of nitromethane under low hydrostatic pressures would be interesting in order to discriminate theses EOS.

3.2.5. Isothermal compressibility β_T

The isothermal compressibility is reported in Fig. 9. A good overall agreement is achieved. When approching the initial state, a slight discrepancy is observed. This is mainly due to the small difference of specific volume at the initial state. The experimental value obtained by Crouzet et al. [9] is 0.8818 $cm^3\ g^{-1}$, the value obtained by Lysne and Hardesty is 0.8935 $cm^3\ g^{-1}$ (+1.3%) and our own simulation result is 0.8741 $cm^3\ g^{-1}$ (−0.9%). If β_T is plotted as a function of v/v_0, the three curves match perfectly.

3.2.6. Coefficient of thermal pressure $(\partial P/\partial T)_V$

As previously observed for Grüneisen parameter, results for the coefficient of thermal pressure, reported in Fig. 10, are notably different (uncertainty decreses from 4.2% to 3.9%). More precisely, the values obtained with the EOS of the literature can vary up to 25%. One can also note that the curve of Lysne and Hardesty and our own results are rather smooth compared to the results of Winey et al. Nonetheless, the magnitudes are of the same order. The lack of experimental results precludes any conclusion about the accuracy of the EOS and of our own results, yet as we mentioned earlier in Section 3.2.3, we are rather trustful in simulation results.

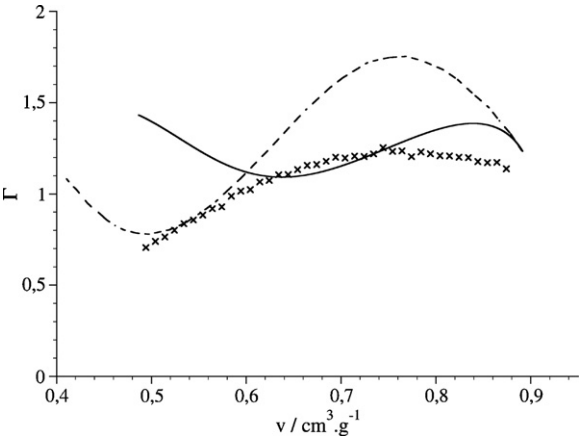

Fig. 7. Grüneisen parameter along the Hugoniot. Same legend as Fig. 1. Simulation uncertainties mentioned in text.

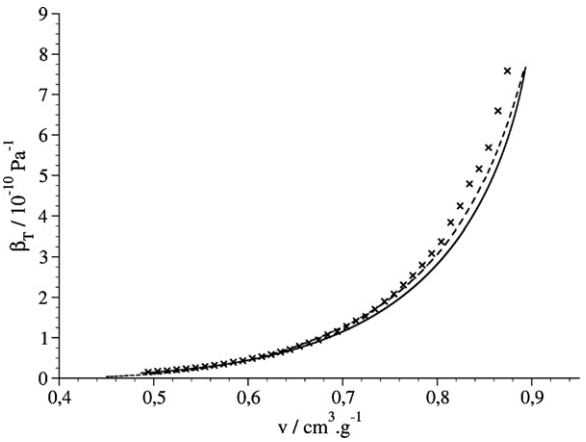

Fig. 9. Isothermal compressibility along the Hugoniot. Same legend as Fig. 1.

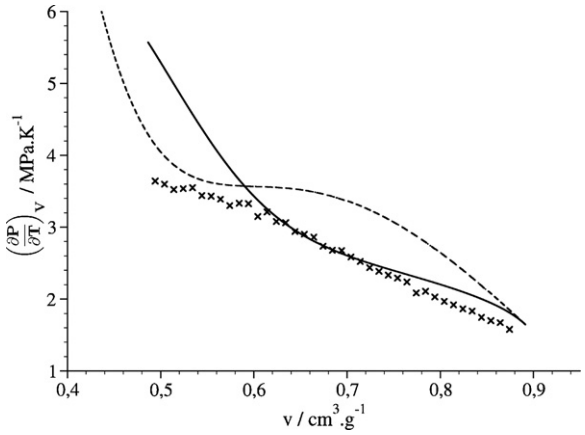

Fig. 10. Coefficient of thermal pressure along the Hugoniot. Same legend as Fig. 1. Simulation uncertainties mentioned in text.

3.2.7. Entropy S

Computing the entropy by molecular simulation is particularly difficult. In this work, we only make use of a differential equation to compute the entropy. This equation (Eq. (8)) is deduced from thermodynamical identities [12,33] and governs the variation of the entropy along the Hugoniot. As each term in this equation is known, S can easily be computed. We have to mention here that entropy in this work is the only quantity which is not based on microscopic considerations. It slightly lowers the reliability of this quantity compared to all the others. The result is reported in Fig. 11 and compared to the EOS of Lysne and Hardesty [12](the same reference of entropy has been taken, see Eq. (13) of Ref. [12]):

$$\left(\frac{\partial S}{\partial v}\right)_H = \frac{P - P_0 + (v_0 - v)(\partial P/\partial v)_H}{2T} \quad (8)$$

3.2.8. Interpolation of the thermodynamic quantities

Interpolation functions of the quantities computed above along the Hugoniot have been deduced from the simulation results. The boundaries of these interpolation functions are reported in Table 4. These relations are supposed to be used in hydrodynamic codes in the near future.

Quantities are as follows: P in GPa, v in cm^3 g^{-1}, $\eta = v/v_0$, T in K, D and u in m s^{-1}, C_v in kJ kg^{-1} K^{-1}, C_s in km s^{-1}, α_P in 10^{-4} K^{-1}, β_T in 10^{-10} Pa^{-1}, $(\partial P/\partial T)_V$ in MPa K^{-1} and S in kJ kg^{-1} K^{-1}:

$$P = 5953.3 \cdot e^{-12.227 \cdot v} - 0.50986 \cdot v^{8.9546}$$

$$P = 5953.73 \cdot e^{-10.688 \cdot \eta} - 0.15285 \cdot \eta^{8.9546}$$

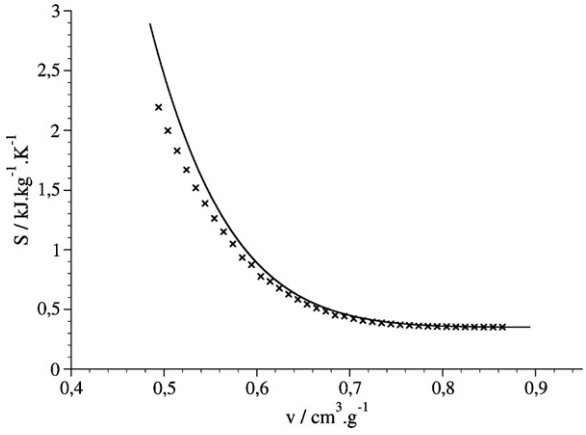

Fig. 11. Entropy along the Hugoniot. Same legend as Fig. 1.

Table 4
Boundaries of the interpolation functions along the Hugoniot.

	Minimum	Maximum
Specific volume v (cm^3 g^{-1})	0.4941	0.8741
Compression η	0.56527	1
Pressure P (GPa)	0	14.21
Temperature T (K)	300	1360.6
Particle velocity u (m s^{-1})	0	2323.7

$$P = -1.391 + 0.0111 \cdot T + 8.785 \times 10^{-7} \cdot T^2 - \frac{1783.79}{T} + \frac{353198}{T^2}$$

$$T = 366.132 - 108.43 \cdot v + \frac{14.275}{v^{6.1}}$$

$$D = 1358.48 + 2.0 \cdot u - 1.258 \times 10^{-4} \cdot u^2$$

$$C_v = 7.858 - 15.036 \cdot v + 8.5479 \cdot v^2$$

$$C_s = -9.4236 + 3.602 \cdot v + \frac{6.6287}{v}$$

$$\Gamma = -2.9674 + 10.907 \cdot v - 7.0904 \cdot v^2$$

$$\alpha_P = -2.695 + 6.327 \cdot v + 26.14 \cdot v^{8.125}$$

$$\beta_T = -0.808 + 1.871 \cdot v + 23.638 \cdot v^{9.826}$$

$$\left(\frac{\partial P}{\partial T}\right)_V = 4.01 + 12.01 \cdot v^{6.68} - 13.79 \cdot v^{4.796}$$

$$S = -23.1 + 37.073 \cdot v - 16.67 \cdot v^2 + \frac{2.93}{v^{1.9}}$$

4. Conclusions

For the first time to our knowledge, a complete equation of state of unreactive shocked liquid nitromethane has been developed from Monte Carlo molecular simulations. It has been previously shown that pressure vs specific volume and shock velocity vs particle velocity are in close agreement with experimental results. Moreover, shock temperatures are in fair agreement with the EOS of Lysne and Hardesty and Winey et al., and second shock temperatures are also consistent with experiments. This last result is of particular interest since up to now no other classical force field of the literature could reproduce quantitatively these shock temperatures while accurate temperature prediction is crucial for thermally activated processes such as chemical reactions.

In a second step, we have computed derivative properties such as the Grüneisen parameter, the heat capacity at constant volume, the sound velocity and others, and a comparaison has been made with two well-known EOS of the literature. Depending on the quantity in question, the agreement between the three EOS varies notably. Sound speed C_s, Isothermal compressibility β_T and coefficient of thermal expansion α_P computed by the two EOS and our Monte Carlo simulations agree with each other. On the contrary, the Grüneisen parameter and the coefficient of thermal pressure $(\partial P/\partial T)_V$ are quite different. Up to now, there is no experimental data that could infer that one of the EOS is much more accurate than another. Nonetheless the transferability of our potential has been checked on second shock temperatures which is known to be a severe test for the quality of a force field. Moreover, we are rather confident in our simulation results since whatever the pressure and

temperature are, the way we compute the derivative properties is the same. On the contrary, the EOS of Lysne and Hardesty and Winey et al. are based on integration schemes which could possibly propagate and accumulate errors on derivative properties, although the EOS of Winey et al. is accurate on second shock temperatures.

In order to get a deeper view of the properties of nitromethane, Molecular Dynamic simulations are currently in progress to study the dynamical properties of nitromethane together with Monte Carlo simulations on a network of isochores to study the behaviour of $(\partial P/\partial T)_V$ and Γ as functions of v and T. At last, MC simulations are considered to study the liquid vapor phase equilibrium (boiling point, saturation pressure) and the solid phase properties of nitromethane. Future prospects are ongoing on isentropic expansions of detonation products.

Acknowledgements

B. Crouzet is gratefully acknowledged for fruitful discussions about the experiments. J.M. Winey is gratefully acknowledged for providing us data points of his EOS and for fruitful discussions. All Monte Carlo simulations have been performed with the Gibbs code from IFP, CNRS and the Université Paris-Sud [41].

References

[1] R.F. Chaiken, The kinetic theory of detonation of high explosives, Master's thesis, Polytechnic Inst. of Brooklin, 1957.
[2] A.N. Dremin, Toward Detonation Theory, Springer Verlag, 1999.
[3] A.W. Campbell, W.C. Davies, J.R. Travis, Shock initiation of detonation in liquid explosives, Phys. Fluids 4 (1961) 498.
[4] D.R. Hardesty, An investigation of the shock initiation of liquid nitromethane, Combust. Flame 27 (1976) 229.
[5] D.A. Frank-Kamenetskii, Diffusion and Heat Exchange in Chemical Kinetics, Plenum Press, 1969.
[6] A. Delpuech, A. Menil, Raman scattering temperature measurement behind a shock wave, APS Shock Waves Conden. Matter (1983) 309.
[7] J.M. Winey, G.E. Duvall, M.D. Knudson, Y.M. Gupta, Equation of state and temperature measurements for shocked nitromethane, J. Chem. Phys. 113 (2000) 7492.
[8] S. Dufort, Mesures de températures sous choc par diffusion raman, J. Phys. C 4 (1987) 137.
[9] B. Léal-Crouzet, G. Baudin, H.N. Presles, Shock initiation of detonation in nitromethane, Combust. Flame 122 (2000) 463.
[10] V. Bouyer, I. Darbord, P. Hervé, G. Baudin, C.L. Gallic, F. Clément, G. Chavent, Shock-to-detonation transition of nitromethane: time-resolved emission spectroscopy measurements, Combust. Flame 127 (2007) 084513.
[11] Y. Gruzdkov, Y. Gupta, Mechanism of amine sensitization in shocked nitromethane, J. Phys. Chem. A 102 (1998) 2322.
[12] P.C. Lysne, D.R. Hardesty, Fundamental equation of state of liquid nitromethane to 100 kbar, J. Chem. Phys. 59 (1973) 6512.
[13] N. Desbiens, E. Bourasseau, J.-B. Maillet, Potential optimization for the calculation of shocked liquid nitromethane properties, Mol. Sim. 33 (2007) 1061.
[14] A. Hervou'ét, N. Desbiens, E. Bourasseau, J.-B. Maillet, Microscopic approaches to liquid nitromethane detonation properties, J. Phys. Chem. B 112 (2008) 5070.
[15] H. Liu, J. Zhao, D. Wei, Z. Gong, Structural and vibrational properties of solid nitromethane under high pressure by density functional theory, J. Chem. Phys. 124 (2006) 124501.
[16] M.L. Price, D. Ostrovsky, W.L. Jorgensen, Gas-phase and liquid-state properties of esters, nitriles, and nitro compounds with the OPLS-AA force field, J. Comp. Chem. 22 (2001) 1340.
[17] P. Ungerer, C. Beauvais, J. Delhommelle, A. Boutin, A. Fuchs, Optimization of the anisotropic united atoms intermolecular potential for *n*-alkanes, J. Chem. Phys. 112 (2000) 5499.
[18] B. Crouzet, D. Partouche-Sebban, N. Carion, Temperature measurements in shocked nitromethane, APS Shock Compress. Conden. Matter (2004) 1253.
[19] E. Bourasseau, J.-B. Maillet, Parameter optimization for charge equilibration method in molecular simulations, APS Shock Compress. Conden. Matter (2005) 565.
[20] H. Liu, J. Zhao, G. Ji, Z. Gong, D. Wei, Compressibility of liquid nitromethane in the high-pressure regime, Physica B 382 (2006) 334.
[21] D.C. Sorescu, B.M. Rice, D.L. Thompson, Intermolecular potential for the hexahydro-1,3,5-trinitro-1,3,5-s-triazine crystal (rdx): a crystal packing, Monte Carlo, and molecular dynamics study, J. Phys. Chem. B 101 (1997) 798.
[22] D.C. Sorescu, B.M. Rice, D.L. Thompson, Theoretical studies of solid nitromethane, J. Phys. Chem. B 104 (2000) 8406.
[23] D.C. Sorescu, B.M. Rice, D.L. Thompson, Molecular dynamics simulations of liquid nitromethane, J. Phys. Chem. A 105 (41) (2001) 9336.
[24] P.M. Agrawal, B.M. Rice, D.L. Thompson, Molecular dynamics study of the melting of nitromethane, J. Chem. Phys. 119 (2003) 9617.
[25] J.M. Seminario, M.C. Concha, P. Politzer, A density functional/molecular dynamics study of the structure of liquid nitromethane, J. Chem. Phys. 102 (20) (1995) 8281.
[26] A.E. Alper, F. Abu-Awwad, P. Politzer, Molecular dynamics simulations of liquid nitromethane, J. Phys. Chem. B 103 (44) (1999) 9738.
[27] H.D. Jones, Equation of state for liquid nitromethane at high pressures, APS Shock Compress. Conden. Matter (2004) 149.
[28] L. Soulard, Shock polar calculation of inert nitromethane by molecular dynamics simulation, APS Shock Compress. Conden. Matter (2002) 173.
[29] E. Bourasseau, V. Dubois, N. Desbiens, J.-B. Maillet, Molecular simulations of hugoniots of detonation product mixtures at chemical equilibrium: Microscopic calculation of the Chapman Jouguet state, J. Chem. Phys. 127 (2007) 084513.
[30] J.K. Brennan, B.M. Rice, Effcient determination of Hugoniot states using classical molecular simulation techniques, Mol. Phys. 101 (2003) 3309.
[31] M. Lagache, P. Ungerer, A. Boutin, A.H. Fuchs, Prediction of thermodynamic derivative properties of fluids by Monte Carlo simulation, Phys. Chem. Chem. Phys. 3 (2001) 4333–4339.
[32] C. Colina, E.A. Muller, Joule-Thomson inversion curves by molecular simulation, Mol. Sim. 19 (1997) 237.
[33] R. Menikoff, B.J. Plohr, The Riemann problem for fluid flow of real materials, Rev. Mod. Phys. 61 (1989) 75.
[34] A. Burcat, B. Ruscic, Third millennium ideal gas and condensed phase thermochemical database for combustion with updates from active thermochemical tables, Tech. Re ANL-05/20 and TAE 960, Technion-IIT, Aerospace Engineering, and Argonne National Laboratory, Chemistry Division, 2005; ftp://ftp.technion.ac.il/pub/supported/aetdd/thermodynamics/.
[35] M. Allen, D. Tildesley, Computer Simulation of Liquids, Clarendon Press, 1987.
[36] S.P. Marsh, LASL Shock Hugoniot Data, University of California Press, 1980.
[37] P. Klébert, Etude expérimentale et théorique de la transition choc détonation dans les explosifs homogénes, PhD thesis, Université Paris VI - Pierre et Marie Curie, 1998.
[38] W.M. Jones, W.F. Giauque, The entropy of nitromethane, heat capacity of solid and liquid, vapor pressure, heats of fusion and vaporization, J. Am. Chem. Soc. 69 (1947) 983.
[39] H.A. Berman, E.D. West, Heat capacity of liquid nitromethane from 35 °C to 200 °C, J. Chem. Eng. Data 14 (1969) 107.
[40] P.W. Bridgman, Theoretically interesting aspects of high pressure phenomena, Rev. Mod. Phys. 7 (1935) 1.
[41] P. Ungerer, A. Boutin, B. Tavitian, Applications of Molecular Simulation in the Oil and Gas Industry, IFP Publications, 2005.